Design and Optimization of Optical Mode Exchange Based on Cascaded Multimode Interferences

Linh Duc Tam Ho[1,3], Duy Quang Duong[2], Dung Cao Truong[2], Quynh Nguyen Quang Nhu[1], Hung Nguyen Tan[1]
[1]*The University of Danang - University of Science and Technology, Danang, Vietnam*
[2]*Posts and Telecomunications Institute of Technology, Hanoi, Vietnam*
[3]*Hue University of Sciences, Hue, Vietnam*
Email: hung.nguyen@dut.udn.vn

***Abstract*—This paper presents a structure realizing an optical mode exchange function using three multimode interferences on silicon-on-insulator substrate, and optimized its performance through 3D beam propagation method simulation with effective index method. Simulations demonstrate a successful exchange of two mode TE0 and TE1 with only 0.38 power loss and small crosstalk of -19 dB within a whole C band. Furthermore, large fabrication tolerance is also an advantage of the device. We believe that the proposed optical mode exchange would be used as an important component to improve the flexibility and efficiency of optical networks using mode-division multiplexing.**

Keywords—mode exchange (ME), mode division multiplexing (MDM), multimode interference (MMI), phase shifter (PS)

I. INTRODUCTION

Optical fiber communications have used different signal multiplexing technologies to increase the data capacity, such as wavelength division multiplexing (WDM), time division multiplexing (TDM), polarization division multiplexing (PDM), quadrature amplitude modulation/multiplexing (QAM), making full use of frequency/wavelength, time, polarization, quadrature of the optical carrier [1]. To further scale the data rates and transmission capacities, another physical dimension of light which is optical mode has also been studied to form the so-call mode division multiplexing (MDM) [2-4]. Because signals are modulated on orthogonal eigenmodes of the light, they can be multiplexed or demultiplexed without interchannel crosstalk, and therefore, the total data capacity could be multiplied with the number of modes [5]. Moreover, MDM based on the platform of silicon photonics integration [6] has opened a new paradigm for on-chip data communications with great improvement in terms of power efficiency, performance and cost thanks to the wide band, low loss, small-crosstalk, small-footprint, high refractive index contrast, and compatibility with matured complementary metal-oxide-semiconductor (CMOS) technologies of the silicon waveguides.

Integrated MDM works have been well focused on the realization of basic elements with simple functionalities such as optical mode multiplexing/demultiplexing or mode conversion (see Fig.1(a)) [7-13]. Other higher functionality elements have also proposed to perform optical mode switching [14] or optical 90 degree hybrids [15-16]. Optical mode exchange (see Fig.1(b)) which allows an all-optical data swapping between two different modes is also a desirable function to improve the flexibility and efficiency of MDM-based networks. Three designs have been proposed to realize the optical mode exchange, based on tapered directional coupler [17], Y-junction [18] and micro-ring resonators (MRRs) [19].

In this paper, we propound a new design of an optical mode exchange based on three cascaded multimode interferences (MMI) built on silicon-on-insulator (SOI) substrates. Lights on modes TE0 and TE1 are, respectively, successfully converted simultaneously to modes TE1 and TE0. The device is designed and optimized through numerical simulation using three dimensional beam propagation method (3D-BPM) and effective index method (EIM). Thanks to the use of silicon MMI couplers the proposed device can operate at a low insertion loss of 0.38 dB and a small crosstalk of -19 dB over a large wavelength between 1520 nm and 1570 nm. Our design also exhibit a large fabrication tolerance against chip-size variations while maintaining the desired performance.

II. PRINCIPLE AND DESIGN

A. Basic MMI theory

The operation of a multimode interference (MMI) is based on self-imaging mechanism in a multimode waveguide. Through the propagation and interference along the MMI, a signal is excited and reproduced to a single or multiple images after periodic intervals. The periodic intervals are dependent of the half-beat length L_π. Here, the L_π is defined as the beat length of the two lowest-order modes in the MMI region and it is given by the formula [20]:

$$L_\pi = \frac{4 n_{eff} W_{eff}^2}{3\lambda} \quad \text{with} \quad W_{eff} = W_{MMI} + \frac{\lambda}{\pi}(n_{eff}^2 - n_{clad}^2)^{-1/2} \qquad (1)$$

where W_{eff} is effective width of the MMI region, and λ, W_{MMI}, n_{eff}, n_{clad} is wavelength, width of MMI, effective index and cladding refractive index, respectively. There are two self-imaging mechanisms. One is general interference and the other is restricted interference [21-22]. In these case, MMIs coupler's length is shown in formula (2) and (3) respectively.

$$L_{MMI} = \frac{M}{N}(3L_\pi) \qquad (2)$$

$$L_{MMI} = \frac{M}{4N}(3L_\pi) \qquad (3)$$

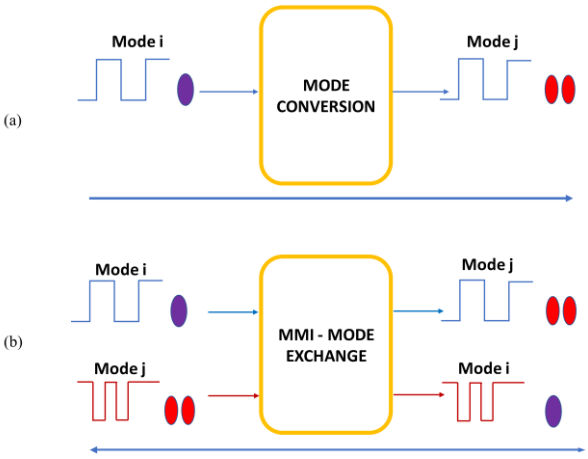

Fig.1. Practical applications of mode exchange: (a) Traditional mode conversion, (b) Mode and data exchange on the same single device.

Where N is the number of input and output ports of the MMI, and M is selectable lengths of MMI's having N output ports. Because MMI's are supposed to be short, we restrict ourselves to cases with M = 1.

Fig.2 shows mode images in a MMI waveguide when the fundamental mode and first order mode is launched into the middle input of it, respectively. At the distance $3L_\pi/4$, the fundamental mode is mapped into the center. On the other hand, the first-order mode is mapped into the edges with different phase π in two arms. But at the distance $3L_\pi/8$, the fundamental mode is mapped into two arms with the same phase. The operation is performed correlate in two converse directions, that means, with $L_{mmi} = 3L_\pi/8$, the two same phase signals TE0 transmitted into the two arms will be reassembled into a TE0 signal at center arm whose the signal amplitude is two times bigger. This property is also completely true for the opposite direction of $L_{mmi} = 3L_\pi/4$.

These phases at the output ports j in relation to the input ports i are given for the general MMI mechanism of Fig.2 with a length L_N, for propagating wave exp(iθ) as by [23]

$$\Delta\phi_{ij} = \phi_0 - \pi - \frac{\pi}{4N}(j-i)(2N-j+i) \text{ for } (i+j)\ even$$
$$\Delta\phi_{ij} = \phi_0 - \frac{\pi}{4N}(j+i-1)(2N-j-i+1) \text{ for } (i+j)\ odd \quad (4)$$

ϕ_0 is an initial constant phase of signals transmitted to waveguide inputs of MMI coupler length L_4 or L_8 in two cases N = 4 or N = 8.

B. *Operating principle*

For TE1 to TE0 conversion, Fig.3(a) illustrates the process mode conversion from a first-order mode TE1 to a fundamental mode TE0. The mode TE1 input signal {i = (2;3)} are separated into two modes TE0 responding at two MMI1's outer arms {j = 1 and j = 4} with π different phase between two arms. After upper arm phase signal is shifted amount of π, two same phase signals placed at MMI2 inputs {i = (2;3) and i = (6;7)} is corresponded to the positions $\pm W_{eff}/4$ with respect to the center of the their region, so a fundamental mode TE0 synthesis signal is shaped in the center outer arm {j = (5;4)}. This desirable mode TE0 is transmitted to MMI3 output {j = (3;2)}. Assuming initial phase $\phi_0 = 0$ and normalized amplitude = 1, from (4), the output signals at stages is showing in the formula below:

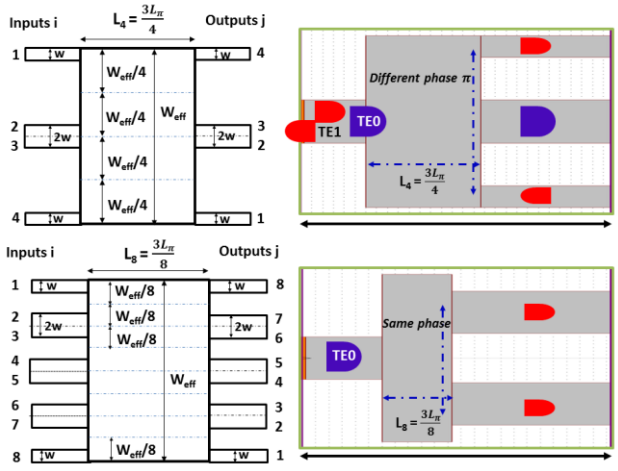

Fig.2. Structure and port indices of MMI $3L_\pi/4$ and $3L_\pi/8$

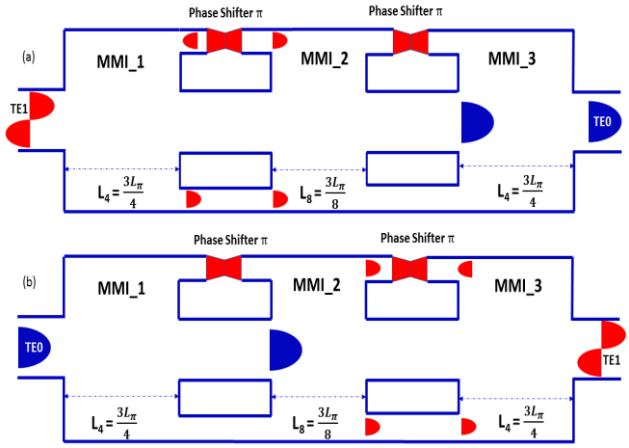

Fig.3. The explanation diagram of the two mode exchange based on MMI waveguide

$$S_{Input} = \begin{pmatrix} 0 \\ 1 \\ 0 \end{pmatrix} e^{i\theta} \rightarrow S_{MMI1} = \frac{1}{\sqrt{2}} \begin{pmatrix} e^{-i\frac{7\pi}{4}} \\ 0 \\ e^{-i\frac{3\pi}{4}} \end{pmatrix} e^{i\theta} \rightarrow$$

$$S_{PS1} = \frac{1}{\sqrt{2}} \begin{pmatrix} e^{-i\frac{3\pi}{4}} \\ 0 \\ e^{-i\frac{3\pi}{4}} \end{pmatrix} e^{i\theta} \rightarrow S_{MMI2} = \begin{pmatrix} 0 \\ e^{-i\frac{21\pi}{8}} \\ 0 \end{pmatrix} e^{i\theta} \rightarrow S_{MMI3} = \begin{pmatrix} 0 \\ e^{-i\frac{29\pi}{8}} \\ 0 \end{pmatrix} e^{i\theta}$$

For TE0 to TE1 conversion, mode conversion from a fundamental TE0 to a first-order mode TE1 is shown in Fig. 3(b). At first, mode TE0 signal at MMI1's input is moved to center arm output {j = (2;3)}. Following MMI2's property with $L_8 = 3L_\pi/8$ length, two fundamental modes TE0 is produced at two upper and lower arms with π phase difference {j = (7;6) and j = (3;2)}. Before being put at the MMI3's input {i = 1 and i = 4}, mode TE0 signal at upper arm is shifted a constantly phase π when through the second phase shifter. Remaining the initial conditions as the first case, output signals at each stage is described by the formula below:

$$S_{Input} = \begin{pmatrix} 0 \\ 1 \\ 0 \end{pmatrix} e^{i\theta} \rightarrow S_{MMI1} = \begin{pmatrix} 0 \\ -\pi \\ 0 \end{pmatrix} e^{i\theta} \rightarrow$$

$$S_{MMI2} = \frac{1}{\sqrt{2}} \begin{pmatrix} e^{-i\frac{23\pi}{8}} \\ 0 \\ e^{-i\frac{23\pi}{8}} \end{pmatrix} e^{i\theta} \rightarrow S_{SP2} = \frac{1}{\sqrt{2}} \begin{pmatrix} e^{-i\frac{15\pi}{8}} \\ 0 \\ e^{-i\frac{-23\pi}{8}} \end{pmatrix} e^{i\theta} \rightarrow S_{MMI3} = \begin{pmatrix} 0 \\ e^{-i\frac{29\pi}{8}} \\ 0 \end{pmatrix} e^{i\theta}$$

C. Structure design

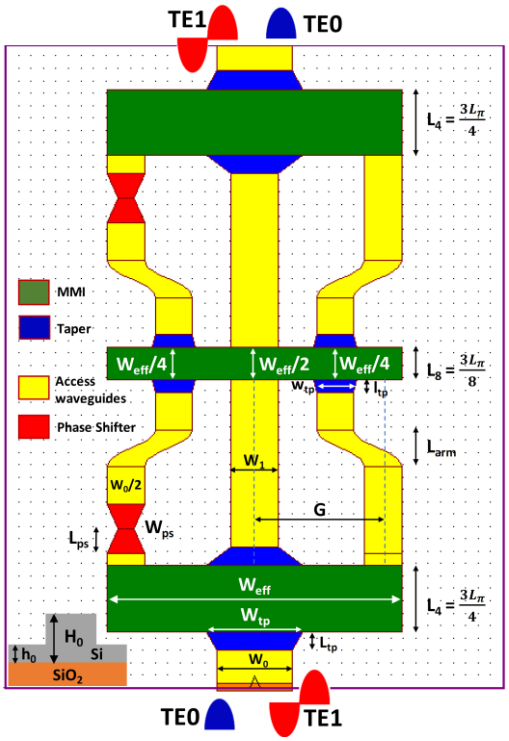

Fig.4. Schematic of the mode exchange based on rid silicon waveguide.

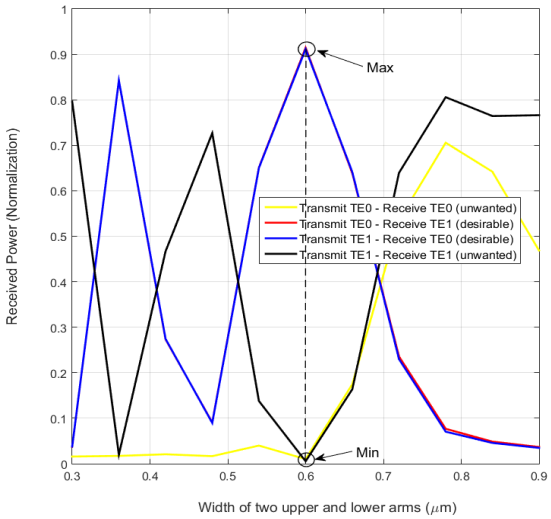

Fig.5. Normalized received power as a function of the two upper and lower arms width.

Here, we describe how to design the parameters of mode exchange device as shown in Fig.4, rib waveguide structures have the slab height h_0 = 220 nm and the height H_0 = 500 nm. We select the materials of the core is Si with a refractive index of 3.45 and SiO_2 with a refractive index of 1.46 for both cladding and upper cover layer. To satisfy transmission two mode TE0 and TE1 at wavelength λ=1550 nm, the center input waveguide w_0 is determined with an appropriate width by beam propagation mode solver, w_0 = 1.2 µm.

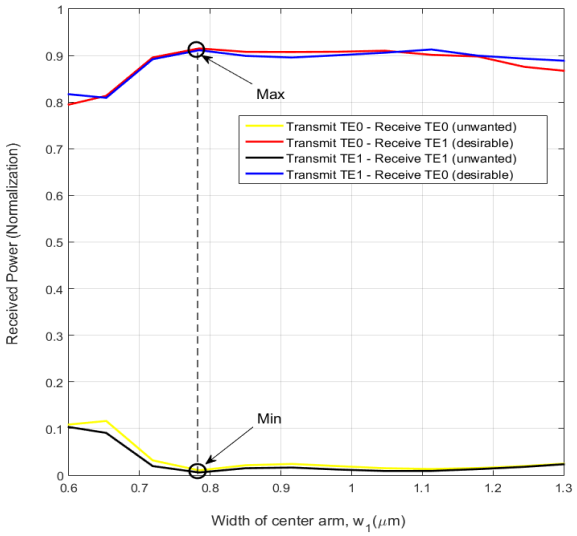

Fig.6. Normalized received power as a function of the center arms width.

From Fig.2, it is obvious that MMI's center input/output waveguides width $L_4 = 3L_\pi/4$ is always double the width of two upper and lower waveguides (see Fig.5). However, to reduce the unwanted coupler effect, we run optimize program to find out the best value, w_1 = 0.78 µm (see Fig.6). In addition, the width of the MMI region defined as W_{MMI} at three MMI couplers are 4.8µm, but the lengths L_{MMI} at MMI couplers are different, particularly, length of MMI coupler L_4 = 53.2 µm is twice compared to length of L_8 = 26.6 µm.

Moreover, a taper is introduced between the input/output waveguide and MMI region to improve the transmission characteristics [24]. We set the width and length of the tapers: W_{tp} = 1.55 µm, w_{tp} = 0.7 µm, l_{tp} = 10 µm and L_{tp} = 15 µm. Furthermore, two important other parameters are also considered in terms of design, those are G = 2.075 µm and L_{arm} = 30 µm (Fig.4), bending access waveguide and bending arm lengths, respectively.

III. Performance Evaluation And Discussion

Fig.7 illustrates field distributions of mode exchange at a wavelength of 1550 nm when launching the fundamental mode and first-order mode at central input. The results show that the distribution of mode fields are completely suitable with theory as presented in the previous parts. Next, Fig.8 shows butterfly shaped phase shifter and phase is changed when mode signal goes through it. We examine phase signals at left arm and right arm output of MMI1. Before the phase signal at MMI1's left arm does not pass through the phase shifter, the phase of the two signals in the two arm are always different amount of π, but after the phase shifters π is placed in the left arm, there is the same phase between the two arms.

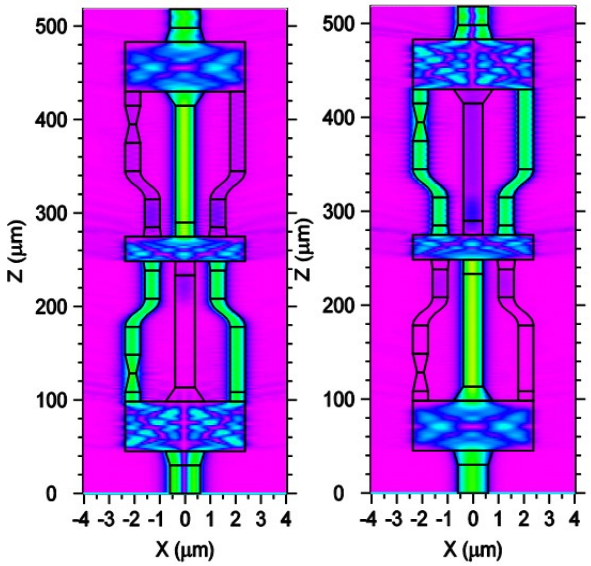

Fig.7. Simulated electric distributions: transmit TE1 - receive TE0 and transmit TE0 - receive TE1, respectively.

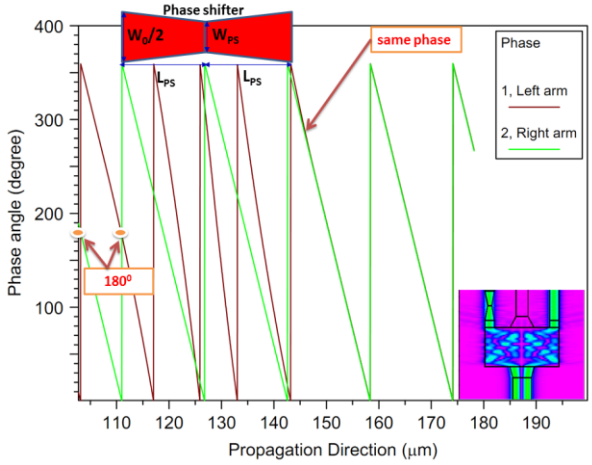

Fig.8. Butterfly shaped phase shifter structure and signal's phase change when transmitting through it.

From Fig.9, we obtain the variation of the normalized received power (normalization) as a function of the central width Wps and there are two width Wps at values 0.26 μm and 0.456 μm to achieve the greatest conversion efficiency.

Two important parameters are insertion loss (IL) and crosstalk (CT) used to evaluate mode conversion performance of proposed device which are defined by:

$$Insertloss = 10\log_{10}\left(\frac{P_{out\_desirable}}{P_{in}}\right) \quad (5)$$

$$Crosstalk = 10\log_{10}\left(\frac{P_{out\_unwanted}}{P_{out\_desirable}}\right) \quad (6)$$

Where P_{in} is the input power of a mode to the waveguide, $P_{out\text{-}desirable}$ is the output power of the desired signal, and $P_{out\text{-}unwanted}$ is the crosstalk power form other modes.

Fig.10 shows the insertion loss and the crosstalk (inset) as functions of wavelength. In this simulation, TE0 and TE1

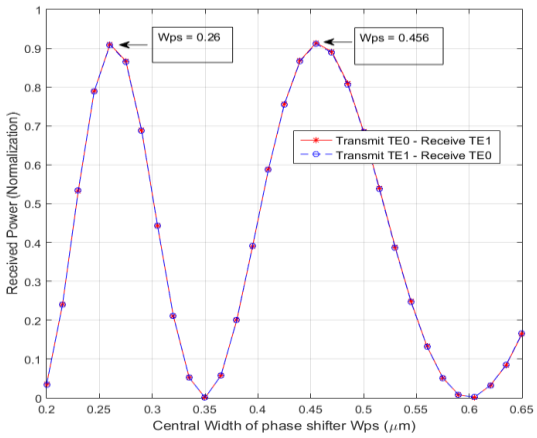

Fig.9. Normalized received power as a function of the central width Wps.

modes are launched one by one. We varied wavelength from 1520 nm to 1570 nm. We observed a small insertion loss and crosstalk that are below 0.85 dB and -19 dB, respectively, within 50 nm wavelength spectra over C standard band.

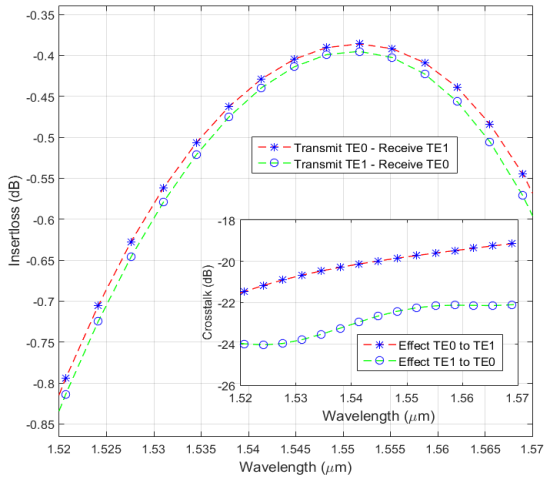

Fig.10. Insertion loss and crosstalk as a function of operation wavelength of mode exchange device TE0 - TE1

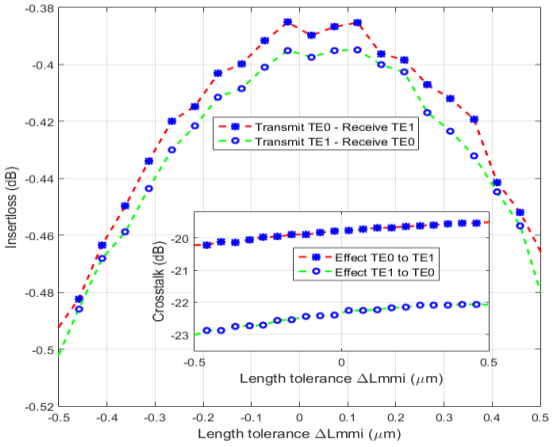

Fig.11. Fabricated tolerances of proposed structure's L_{mmi} coupler length

In the next stage, we examine the effect of manufacture inaccuracy to optical mode conversion performance of the

device. Firstly, we evaluate the fabrication errors to the length of MMI as shown in Fig.11. We see that the length L_{MMI} varies within a range of ± 0.5 µm, the two evaluated parameters IL and CT of the proposed structure are below 0.5 dB and -19.5 dB, respectively. Following this, we survey the variation of the etching depth h_0. The thickness of the SOI etching layer is very important when producing real devices. Fig.12 illustrates the IL and CT depending on the etching depth variation. The simulation results give that as the depth of etching layer differ in range ± 5 nm, the value of the CT is smaller than -19 dB while the figure for the IL is below 0.54 dB. These obtained large tolerances of the structure are totally suitable to current manufacture technologies. We also noted that the crosstalk in both cases involved L_{MMI} and h_0 fabrication tolerances, the effect of TE0 to TE1 was always larger than that of TE1 to TE0.

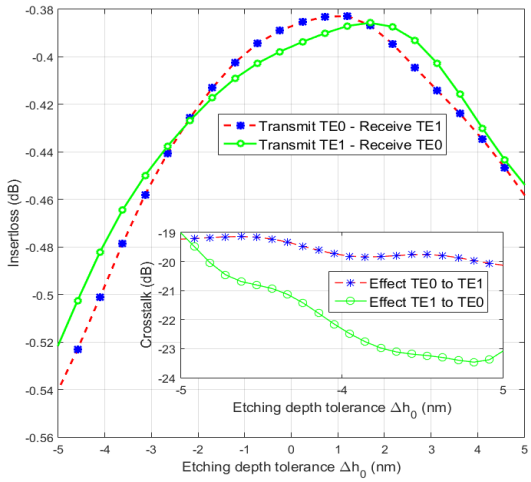

Fig.12. Etching depth tolerances Δh_0 of proposed structure

IV. Conclusion

To summarize, we have proposed a novel photonic integrated circuit performed well mode exchange on Silicon-on-insulator platform with large fabrication tolerance. The consequences present successful mode exchange operations between fundamental mode TE0 and first-order mode TE1 over a wide wavelength range of 50 nm (from 1520 nm to 1570 nm) and achieve a large efficiency approximately 91.5%.

ACKNOWLEDGMENT

This research is funded by Vietnam Ministry of Education and Training under project number B2018.DNA.05

References

[1] E. Agrell, M. Karlsson, A. R. Chraplyvy, D. J. Richardson, P. M. Krummrich, P. Winzer, K. Roberts, J. K. Fischer, S. J. Savory, B. J. Eggleton, M. Secondini, F. R. Kschischang, A. Lord, J. Prat, I. Tomkos, J. E. Bowers, S. Srinivasan, M. Brandt-Pearce, and N. Gisin, "Roadmap of optical communications," J. Opt. 18, 063002 (2016).

[2] S. Berdague and P. Facq, "Mode division multiplexing in optical fiber," Appl. Opt., vol. 21, pp. 1950–1955, 1982.

[3] D. A.B.Miller, "Optical interconnects to silicon chips using short pulses," IEEE J. Sel. Top. Quantum Electron., vol. 6, no. 6, pp. 1312–1317, 2000.

[4] R. Nagarajan et al., "Large-scale photonic integrated circuits," IEEE J. Sel. Top. Quantum Electron., vol. 11, no. 1, pp. 50–65, 2005.

[5] R. Ryf *et al.*, "Mode-division multiplexing over 96 km of few-mode fiber using coherent 6×6 MIMO processing," *J. Light. Technol.*, vol. 30, no. 4, pp. 521–531, 2012.

[6] D. X. Xu et al., "Silicon Photonic Integration Platform—Have We Found the Sweet Spot?," IEEE Journal of Selected Topics in Quantum Electronics, vol. 20, no. 4, pp. 189-205, July-Aug. 2014.

[7] N. Hanzawa *et al.*, "Mode multi/demultiplexing with parallel waveguide for mode division multiplexed transmission," *Opt. Express*, vol. 22, no. 24, pp. 29321–29330, 2014.

[8] W. Chen, P. Wang, and J. Yang, "Mode multi/demultiplexer based on cascaded asymmetric Y-junctions," *Opt. Express*, vol. 21, no. 21, pp. 25113–25119, 2013.

[9] L.-W. Luo *et al.*, "WDM-compatible mode-division multiplexing on a silicon chip," *Nat. Commun.*, vol. 5, no. 3069, pp. 1–7, 2014.

[10] Y. Li, C. Li, C. Li, B. Cheng, and C. Xue, "Compact two-mode (de)multiplexer based on symmetric Y-junction and Multimode interference waveguides," *Opt. Express*, vol. 22, no. 5, p. 5781, 2014.

[11] J. Wang et al, "Improved 8-channel silicon mode demultiplexer with grating polarizers," Opt. Express 22(11), 12799–12807 (2014).

[12] John D. Love and Nicolas Riese, "Single-, Few-, and Multimode Y-Junctions", Journal of Lightwave technology, Vol.30, No.3, Feb 1, 2012.

[13] Fei Guo, Dan Lu, Ruikang Zhang, Huitao Wang, Chen Ji, A Two-Mode (De)Multiplexer Based on Multimode Interferometer Coupler and Y-Junction on InP Substrate, Volume 8, Number 1, February 2016.

[14] B. Stern, et al, "On-chip mode-division multiplexing switch," Optica 2(6), 530–535 (2015).

[15] L. Zimmermann, K. Voigt, G. Winzer, K. Petermann and C. M. Weinert, "C-Band Optical 90°-Hybrids Based on Silicon-on-Insulator 4x4 Waveguide Couplers," *IEEE Photonics Technology Letters*, vol. 21, no. 3, pp. 143-145, Feb.1, 2009.

[16] Hang Guan et al., "Compact and low loss 90° optical hybrid on a silicon-on-insulator platform," Opt. Express 25, 28957-28968 (2017).

[17] Z. Zhang, X. Hu, and J. Wang, "On-chip optical mode exchange using tapered directional coupler," *Nat. Sci. Reports*, vol. 5, no. 16072, pp. 1–8, 2015.

[18] Chunlei Sun, Yu Yu, Guanya Chen, and Xinliang Zhang, "Integrated switchable mode exchange for reconfigurable mode-multiplexing optical networks" vol. 41, no. 14, Optics Letters, July 15 2016.

[19] Mengyuan Ye, et al, "On-chip data exchange for mode division multiplexed signals" Optical Society of America., vol. 24, no. 1, 7 Jan 2016.

[20] R. M Jenkins, R. W. J. Devereux, and J. M. Heateon, "Waveguide beam splitters and recombiners based on multimode propagation phenomena", Opt. Lett., vol. 17, no. 14, pp. 991–993, July 1992.

[21] Lucas B. Soldano and Erik C. M. Pennings, "Optical Multi-Mode Interference Devices Based on Self-Imaging: Principles and Applications", Journal of Lightwave technology, Vol.13, No.4, April, 1995.

[22] M. Bachmann, P. A. Besse, and H. Melchior, "General self-imagingproperties in NxN multimode interference couplers including phase relations", Appl. Opt., vol. 33, pp. 3905–3911, July 1994.

[23] Juerg Leuthold, Juerg Eckner, Emil Gamper, Pierre A. Besse, and Hans Melchior, "Multimode Interference Couplers for the Conversion and Combining of Zero- and First-Order Modes", Journal of Lightwave technology, Vol.16, No.7, July 1998.

[24] J.Xiao, X.Liu, and X.Sum, "Design of an ultracompact MMI wavelength demultiplexer in slot waveguide structures," Opt. Exp., vol. 15, no. 13, pp. 8300–8308, Jun. 2007.